Electronic Supplementary Material (ESI) for Dalton Transactions.

Supporting Information

Table of Contents

	represented here corresponds to a value of 0.03 e^{-}/ $bohr^3$.	

Table S1. Selected Bond Distances (Å) and Bond angles (º) for **1**

Bond Lengths around Dy		Bond Angle	
Dy1- Dy1a	3.7618(4)	Dy1 -O1- Dy1a	107.61(10)
Dy1- O1	2.309(3)	N1a-$^{-}$Dy1- N2a	64.86(12)
Dy1- O1a	2.352(3)	O4-Dy1-O5	70.885(106)
Dy1- O2	2.348(3)	O3a-Dy1a-O2a	70.578(106)
Dy1- O3	2.364(3)		
Dy1- O4	2.353(3)		
Dy1- O5	2.360(3)		

‘a’atoms are generated by the symmetry operation: (1-x,1-y,1-z)

Table S2. Selected Bond Distances (Å) and Bond angles (º) for **2**

Bond Lengths around Dy		Bond Angle	
Dy1- Dy1a	3.7721(8)	Dy1- O1- Dy1a	107.20(10)
Dy1- O1	2.320(3)	N1a- Dy1- N2a	64.61(11)
Dy1- O1a	2.366(3)	O5-Dy1-O4	71.701(100)
Dy1- O2	2.345(3)	O2a-Dy1-O3a	71.639(101)
Dy1- O3	2.336(3)		
Dy1- O4	2.342(3)		
Dy1- O5	2.351(3)		

‘a’atoms are generated by the symmetry operation: (1-x,1-y,1-z)

Table S3. Continuous Shape Measurements for the Dy^{III} ions in **1-3**.

Complex **1**													
Sites	OP-8	HPY-8	HBPY-8	CU-8	SAPR-8	**TDD-8**	JGBF-8	JETBPY-8	JBTPR-8	BTPR-8	JSD-8	TT-8	ETBPY-8
Dy1	32.310	25.081	16.991	10.495	3.177	**0.505**	13.827	30.798	3.357	2.564	3.034	11.318	25.171
Dy2	32.310	25.081	16.991	10.495	3.177	**0.505**	13.827	30.798	3.357	2.564	3.034	11.318	25.171
Complex **2**													
Sites	OP-8	HPY-8	HBPY-8	CU-8	SAPR-8	**TDD-8**	JGBF-8	JETBPY-8	JBTPR-8	BTPR-8	JSD-8	TT-8	ETBPY-8
Dy1	31.928	24.477	17.093	10.404	2.703	**0.544**	13.469	30.647	3.091	2.331	3.020	11.256	24.683
Dy2	31.928	24.477	17.093	10.404	2.703	**0.544**	13.469	30.647	3.091	2.331	3.020	11.256	24.683
Complex **3**													
Sites	OP-8	HPY-8	HBPY-8	CU-8	SAPR-8	**TDD-8**	JGBF-8	JETBPY-8	JBTPR-8	BTPR-8	JSD-8	TT-8	ETBPY-8
Dy1	33.942	20.717	16.208	12.533	4.076	**1.973**	12.822	26.898	3.537	2.938	4.034	12.946	22.631
Dy2	33.030	23.602	15.826	12.667	3.717	**1.324**	11.786	27.384	2.845	2.174	2.958	13.193	24.249

Table S4. Comparison of Bond Angle and Bond Length of Different Dy_2 Complexes.

Metal Complexes	**Dy- $O_{phenoxy}$ (Å)**	**Dy-N $_{imine}$ (Å)**	**Dy-Dy (Å)**	**Dy-$O_{phenoxy}$-Dy(^{0})**	**Ref**
$[Dy^{III}_2(valdien)_2(NO_3)_2]$ [a]	2.31-2.33	2.50-2.52	3.76	108.22	1
$[Dy_2(tfa)_4L_2]$ [b]	2.30-2.37	2.66-2.45	3.81	108.72	2
$[Dy_2((L)_2]\cdot 2CH_3CN$[c]	2.24-2.33	2.49-2.75	3.89	110.4	3
$[Dy_2(MeOH)_2(HL_1)_2(NO_3)_2]\cdot 2MeOH$[d]	2.24	2.46	3.70	110.72	4
$[Dy_2(L)_2(DBM)_2(DMA)_2]\cdot 2DMA\cdot 2CH_3CN$ [e]	2.34	2.48	3.75	105.52	5
$Dy_2(ovph)_2(NO_3)_2(H_2O)_2]_3$ $2H_2O$ [f]	2.17	2.45	3.82	110.12	6
$[Dy^{III}_2(Hhmb)_3(NCS)_3]\cdot 2MeOH\cdot py$, [g]	2.29-2.43	2.54	3.56	96.1	7
[$Dy_2(LH)_2$(μ2-Piv-κ2	2.387	2.501	3.67	100.39	8

O,O′)2(NO3-κ2 O,O′)2] [h]					
$[Dy_2L_3](ClO_4)_3\cdot6CH_3OH$[i]	2.30-2.32	2.56–2.61	3.49	96.86	9
$[Dy_2(acac)_2(L)_2(EtOH)_2]$[j]	2.20–2.40	2.41	3.97	113.01	10
$[Dy_2(L_1)_2(piv)_2]$[k]	2.18-2.42	2.54-2.36	3.78	110.19	11
$[Dy_2(opch)_2(OAc)_2(H_2O)_2]\cdot$ MeOH [l]	2.14- 2.41	2.47-2.56	3.89	113.1	12
$[Dy(tfa)_2(L)]_2$[m]	2.32-2.37	2.45 - 2.68	3.83	109.2	13
$[Dy(LH_3)Cl_2]_2\cdot2Et_2O$[n]	2.28	2.45	3.68	105.51	14

Abbreviations:

a) H_2valdien = *N1,N3*-bis(3-methoxysalicylidene) diethylenetriamine),
b) HL = 2-[((4-bromophenyl)-imino)methyl]-8-hydroxyquinoline, tfa = trifluoroacetylacetonate
c) H_3L= N1,N2,N3,N4-tri(3-methoxysalicylidene) triethylenetetramine
d) H_3L_1= 3-(((2-hydroxynaphthaen-1-yl)methylene)amino)- propane-1,2-diol
e) H2L = 2-(2-hydroxy-3- methoxybenzylideneamino)phenol, HDBM = dibenzoylmethane, DMA = dimethylacetamide,
f) H_2ovph = *N′*-(2-hydroxy-3-methoxybenzylidene)picolinohydrazide
g) H2hmb = N′-(2-hydroxy-3-methoxybenzylidene)benzhydrazide
h) LH2 = N′- (2-hydroxy-3-methoxybenzylidene)acetohydrazide
i) HL= 2,6-diformyl-4-methylphenol di(benzoylhydrazone
j) H2L = N'-(2-hydroxy-5-methylphenyl)-pyrazine-2-carbohydrazide, Hacac = acetylacetone
k) H_2L_1=N_1,N_3-bis(salicylaldehyde)diethylenetriamine
l) H_2opch= (*E*)-*N′*-(2-hydroxy-3-methoxybenzylidene)pyrazine-2-carbohydrazide
m) HL = 2-[[(4-methylphenyl)imino]methyl]-8-hydroxyquinoline
n) LH_4 = 2,3-dihydroxybenzylidene)-2-(hydroxyimino)propanehydrazide

Table S5. Selected Bond Distances (Å) and Bond angles (⁰) for **3**

Bond Lengths around Dy		Bond Angle	
Dy1- Dy2	3.8422(6)	Dy1- O1- Dy2	109.16(19)
Dy1- O1	2.423(5)	Dy1- O6- Dy2	110.21(19)
Dy1- O6	2.333(5)	O2-Dy1-O3	71.892(221)
Dy1- O3	2.266(6)	O4-Dy2-O5	71.253(213)
Dy1- O4	2.359(7)		
Dy1- O5	2.285(6)		
Dy2- O1	2.291(5)		
Dy2- O6	2.351(5)		
Dy2- O8	2.277(5)		
Dy2- O7	2.253(5)		
Dy2- O9	2.438(6)		

Table S6. Table S6. Fitted exchange coupling constants, J^{exch} (cm^{-1}), for 1-3 and the Reported Phenoxido-Bridged Dy_2 Complexes

Dy_2 Complex	Dy-Dy (A⁰)	<Dy-O-Dy (⁰)	$J_{exchange}$	U_{eff}/K and Relaxation time (τ_0)/s	ref
$[Dy_2(a'povh)_2(OAc)_2(DMF)_2]^a$	3.67	102.62	-8.375	322.1 K, $\tau_0 = 3.4 \times 10^{-9}$	15
$[Dy_2(nb)_4(H_3L)_2]^b$	3.69	105.24	-2.75	290.1 K, $\tau_0 = 5.54 \times 10^{-12}$	16
$[Dy_2(Pc)_2(L\text{-}OCH_3)_2(H_2O)]\cdot 2THF^c$	3.93	106.4	-1.23	58.8K, $\tau_0 = 1.12 \times 10^{-8}$	17
$[Dy_2(L)_2(NO_3)_2(MeOH)_2]^d$	3.72	106.4	−6.00	97.42 K,	18

				$\tau_0 = 2.80 \times 10^{-5}$	
[$Dy_2(LH_1)_2$(tfa)$_4$]	**3.77**	**107.198**	**-0.12**	**21.63 K,** **$\tau_0 = 7.32 \times 10^{-6}$**	**This work**
[$Dy_2(LH_1)_2$(hfac)$_4$]	**3.76**	**107.602**	**-0.20**	**9.04 K,** **$\tau_0 = 3.19 \times 10^{-6}$**	**This work**
[Dy_2(valdien)$_2$(NO_3)$_2$][e]	3.76	108.22	-0.21	76 K, $\tau_0 = 6.04 \times 10^{-7}$	1
[Dy_2L(O_2CPh)$_2$]·2MeOH[f]	3.79	108.44°	–1.25	47.51 K, $\tau_0 = 6.42 \times 10^{-6}$	19
Dy_2(dbm)$_2$(LH)$_2$]·H_2O[g]	3.80	109.5	9.49	76.18 K, $\tau_0 = 2.54 \times 10^{-8}$	20
[$Dy_2(L^1)_2$(piv)$_2$][h]	3.79	110.19	−1.50	40.32 K, $\tau_0 = 3.06 \times 10^{-6}$	11
[Dy_2(LH1)$_2$(NO_3)(tmhd)$_3$]	**2.38**	**110.25**	**-0.09**	**25.65 K,** **$\tau_0 = 4.86 \times 10^{-5}$**	**This work**
[Dy(acac)$_2$(CH_3OH)]$_2$(μ-HMq)$_2$[i]	3.92	112.71	-0.75	65.3 K, $\tau_0 = 6.3 \times 10^{-8}$	21
[Dy_2(DMOP)$_2$(DBM)$_4$($C_2H_4Cl_2$)$_2$][j]	3.84	113.32	-2.51	147.2 K, $\tau_0 = 2.3 \times 10^{-8}$	22

Abbreviations:

a) H_2a'povh=N'-[amino(pyrimidin-2-yl)methylene]-o-vanilloyl hydrazine)
b) H_3L =2-hydroxyimino-N′-[(2-hydroxy- 3-methoxyphenyl)methylidene] propanohydrazone
   Hnb = m-nitrobenzoic acid
c) H_2Pc = Phthalocyanine, HL-OCH$_3$= 2-hydroxy-3-methoxybenzaldehyde
d) H_2L = 2-(((2-hydroxy-3-methoxybenzyl)imino)methyl)-4-methoxyphenol
e) H_2valdien = *N1,N3*-bis(3-methoxysalicylidene)diethylenetriamine)
f) H_2L=N_1,N_3-bis(4-chlorosalicyladehyde)diethylenetriamine
g) LH_3 = (1*E*,3*E*)-2-hydroxy-5-methylisophthalaldehyde dioxime, Hdbm = dibenzoylmethane
h) H_2L_1=N_1,N_3-bis(salicylaldehyde)diethylenetriamine
i) HMq = 2-methyl-8-hydroxyquinoline, acac = acetylacetone
j) DMOP = 2,6-dimethoxyphenol , DBM = dibenzoylmethane

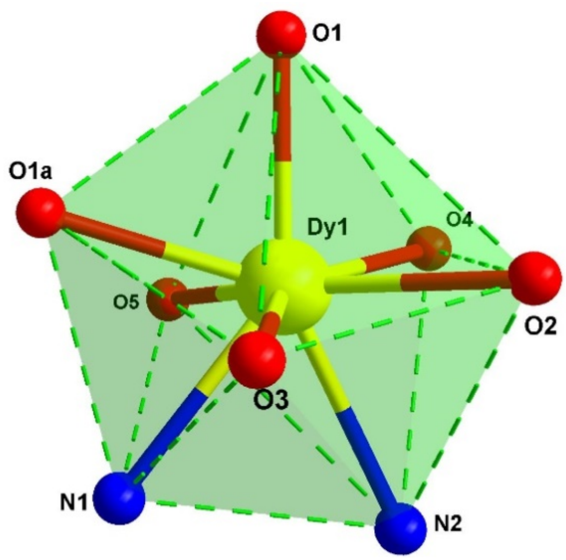

Figure S1. Distorted Trigonal Dodecahedron Geometry

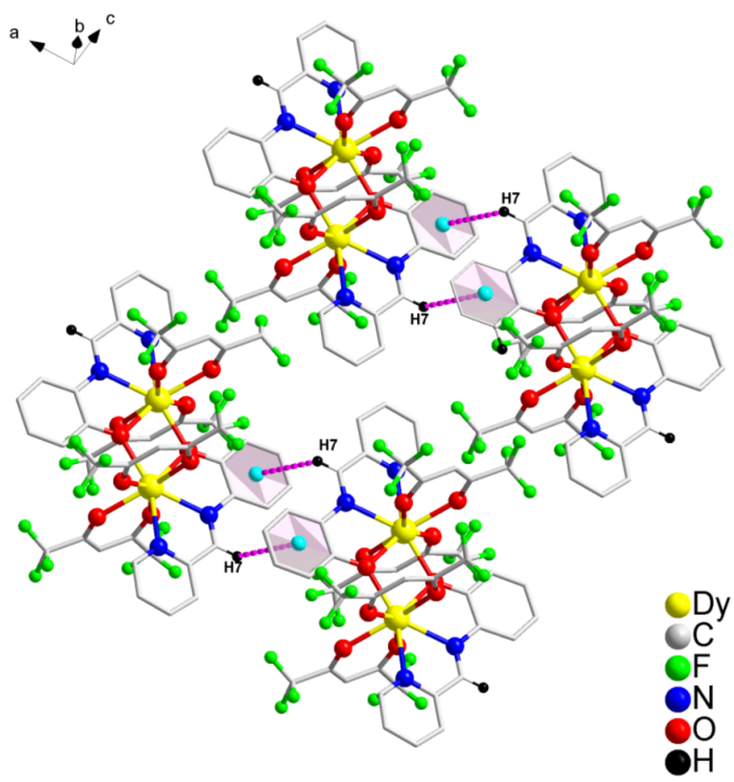

Figure S2. Supramolecular one-dimensional Zigzag Chain for **1**

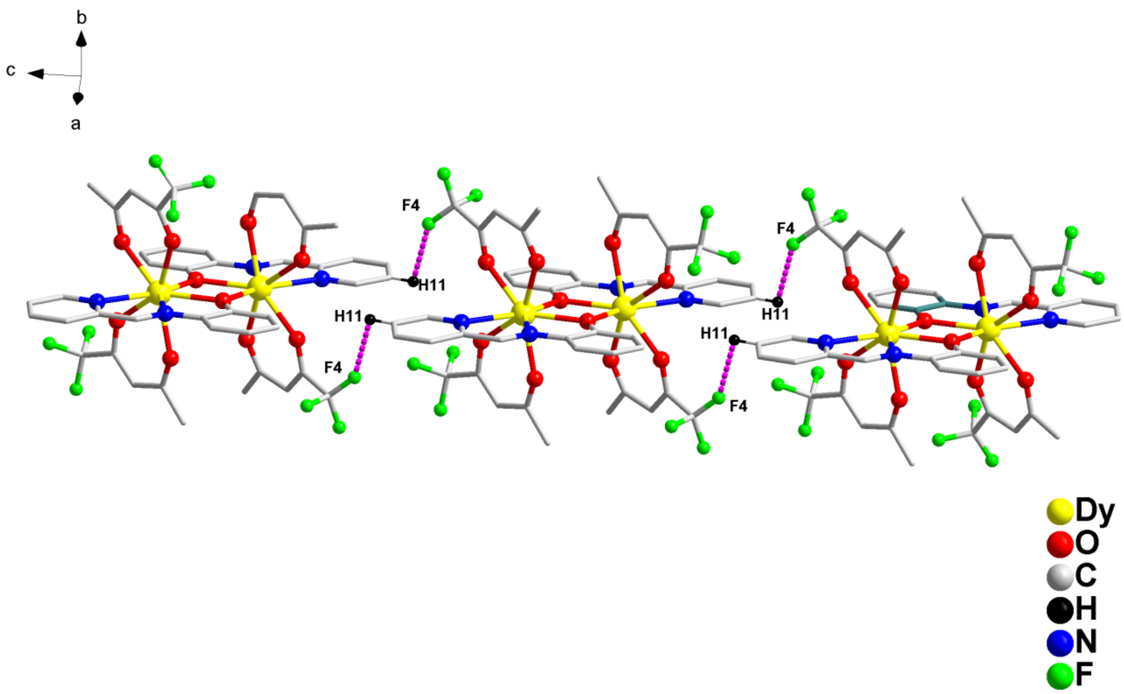

Figure S3. Supramolecular Interaction C-H····F and C-H····π interactions for **2**

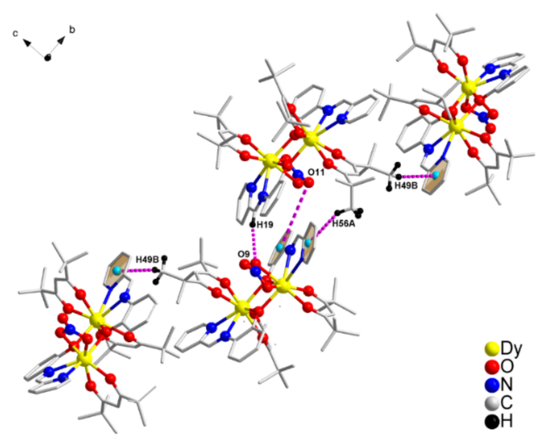

Figure S4. Supramolecular interaction for **3**.

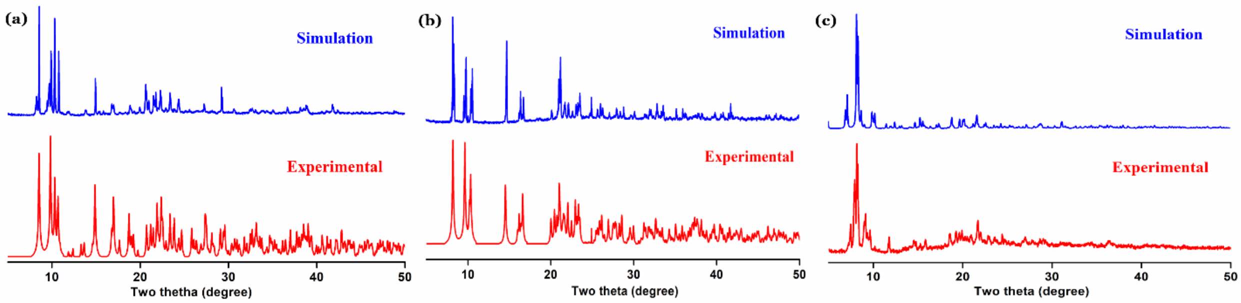

Figure S5. Experimental PXRD patterns and simulated patterns generated from single crystal X-ray diffraction data for complexes 1(a), 2 (b) and 3 (c).

Complex 1 **Complex 2** **Complex 3**

Figure S6. TGA of complexes **1**, **2** and **3**.

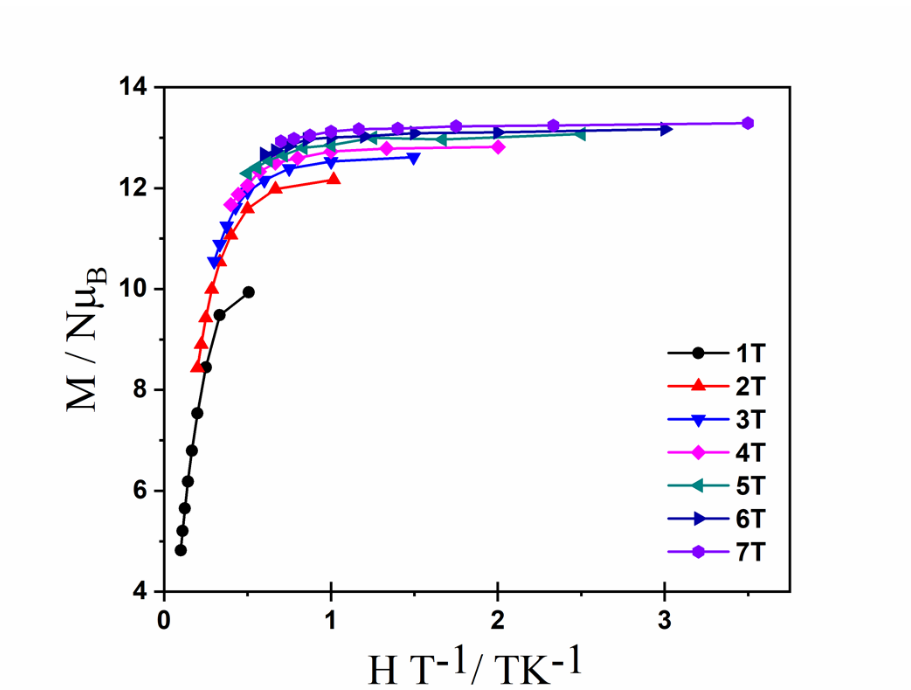

Figure S7. Temperature dependence of the magnetization of **1** at different fields.

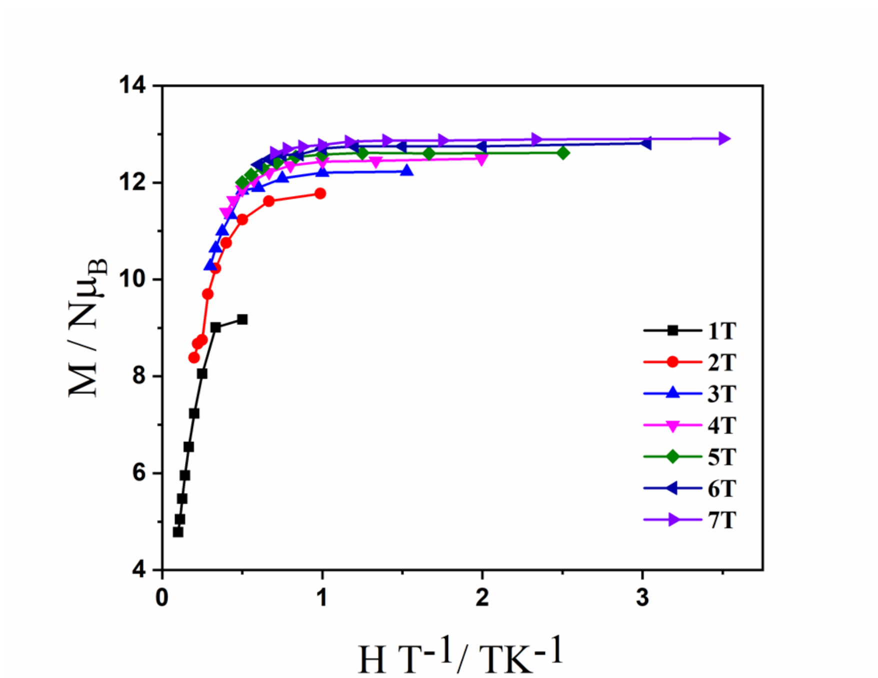

Figure S8. Temperature dependence of the magnetization of **2** at different fields.

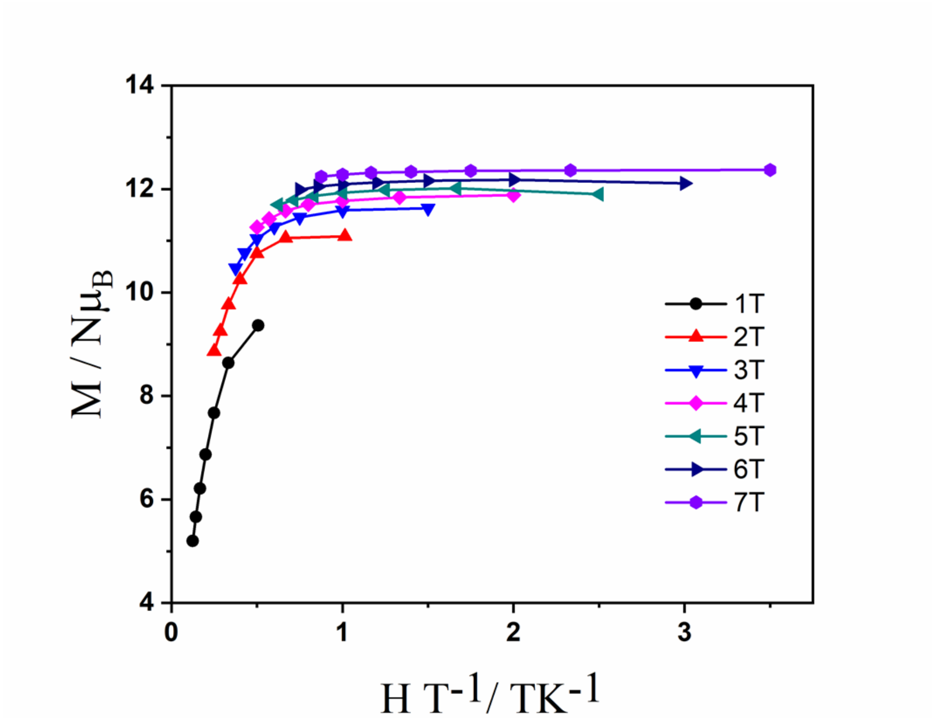

Figure S9. Temperature dependence of the magnetization of **3** at different fields.

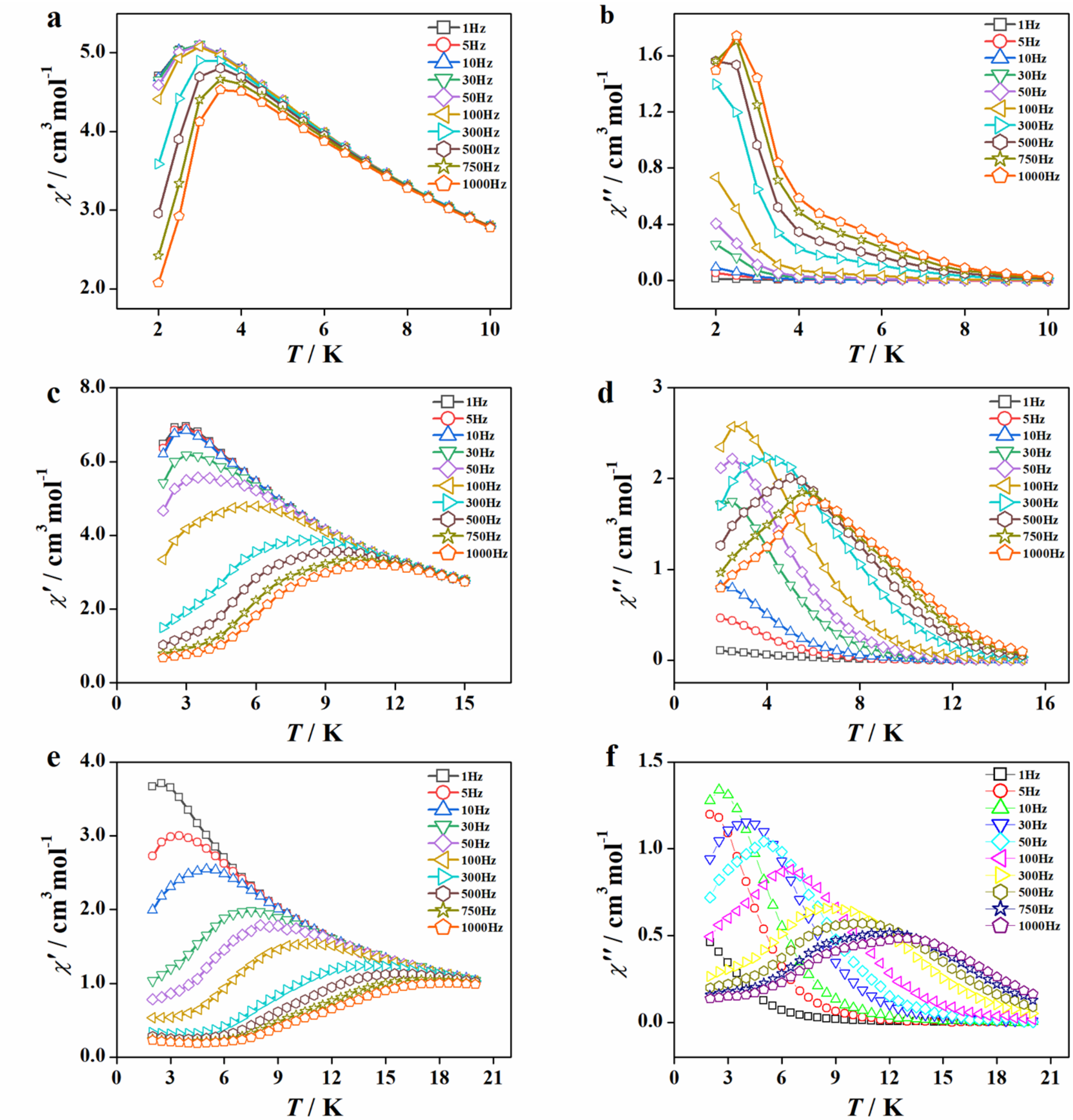

Figure S10. Temperature dependence of the in-phase (left) and out-of-phase (right) ac susceptibilities at the indicated frequency range for complexes **1–3** respectively under the zero field. Plots a and b for **1**, plots c and d for **2**, plots e and f for **3** respectively.

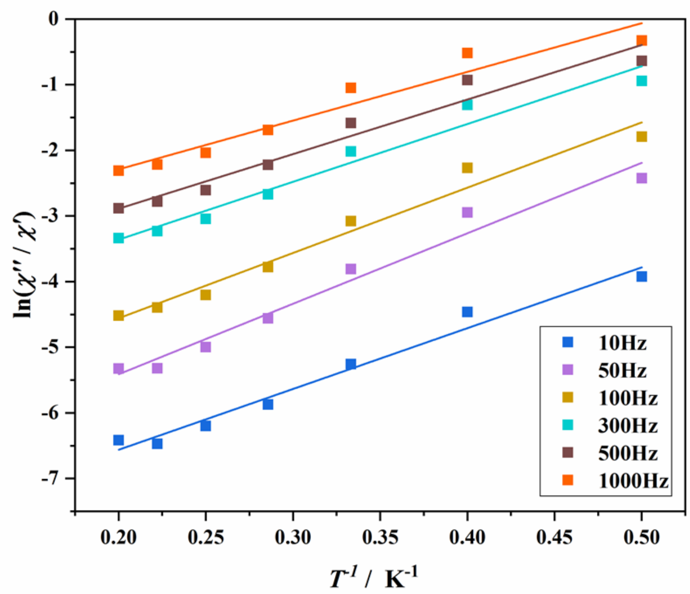

Figure S11. Plots of ln(χ″/χ′) versus 1/T for **1**. The solid line represents the fitting results.

Table S7. Best fitted parameters (χ_T, χ_S, τ and α) with the extended Debye model for complex **2** in the temperature range 2-12 K.

T / K	χ_S/ cm³ mol⁻¹	χ_T / cm³ mol⁻¹	τ / s	α	Residual
2	0.350481E+00	0.665958E+01	0.128883E-02	0.163959E+00	0.607703E-01
3	0.280499E+00	0.630014E+01	0.891005E-03	0.166752E+00	0.107417E+00
4	0.394313E+00	0.606689E+01	0.163415E-02	0.162261E+00	0.517652E-01
5	0.168174E+00	0.572827E+01	0.549796E-03	0.195841E+00	0.125834E+00
6	0.861614E-01	0.520035E+01	0.317335E-03	0.224695E+00	0.184454E+00
7	0.973595E-08	0.479211E+01	0.172517E-03	0.329566E+00	0.885052E+00
8	0.720337E+00	0.429516E+01	0.152362E-03	0.182583E+00	0.111876E+00
9	0.109531E+01	0.392707E+01	0.118928E-03	0.125894E+00	0.364341E-01
10	0.131191E+01	0.361159E+01	0.884013E-04	0.777668E-01	0.860003E-02
11	0.998760E-08	0.343371E+01	0.117237E-04	0.423714E+00	0.600370E+00
12	0.389307E+00	0.311832E+01	0.212144E-04	0.103405E+00	0.896909E-02

Table S8. Best fitted parameters (χ_T, χ_S, τ and α) with the extended Debye model for complex **3** in the temperature range 2-12 K.

T / K	χ_S/ cm³ mol⁻¹	χ_T / cm³ mol⁻¹	τ / s	α	Residual
2	0.182473E+00	0.373421E+01	0.120052E-01	0.217182E+00	0.528326E-01
3	0.213776E+00	0.370381E+01	0.167642E-01	0.246978E+00	0.675996E-01
4	0.161974E+00	0.341734E+01	0.793087E-02	0.196216E+00	0.385585E-01
5	0.142261E+00	0.303111E+01	0.492711E-02	0.183860E+00	0.244681E-01
6	0.127306E+00	0.270785E+01	0.301886E-02	0.180590E+00	0.226791E-01
7	0.117925E+00	0.243810E+01	0.187997E-02	0.187323E+00	0.263958E-01
8	0.130859E+00	0.221769E+01	0.121461E-02	0.191449E+00	0.332745E-01
9	0.172797E+00	0.202096E+01	0.830336E-03	0.180391E+00	0.314681E-01
10	0.329506E-14	0.361752E+01	0.286170E-01	0.775504E+00	0.541527E+01
11	0.254338E+00	0.171447E+01	0.429667E-03	0.144991E+00	0.199198E-01
12	0.189065E-07	0.222463E+01	0.504246E-03	0.752444E+00	0.293394E+01

Computational Details

All the calculations were carried out on the X-ray crystal structure using the MOLCAS 8.0 suite of programs.[23] In order to compute the magnetic property of individual Dy centres, the neighboring Dy ions were replaced by a diamagnetic closed-shell Lu^{3+}. CASSCF/RASSCF, CASPT2, and multistate CASPT2 were performed to extract the Spin Hamiltonian parameters in the complexes.[24-28] All the calculations were performed using an ANO-RCC type basis set[29]. The following contractions were used :

Dy/Lu……. 7s6p4d2f.

C, N, O, F…….. 3s2p.

H…….2s.

The electronic configuration of Dy(III) is $4f^9$, which possesses a ground state term of $^6H_{15/2}$. The active space include 4f shell of Dy^{3+} ion: CAS (9,7), i.e., nine electrons in the seven f-orbitals of

Dy(III). We have computated 21 Spin Free roots of sextate using this active space then we have computed 126 roots of Spin Orbit states by introducing RASSI-SO module[30]. To better understanding of g-tensor orientation, LoProp charges were also computed. In the next step, we took these spin-orbit states in the SINGLE_ANISO module of MOLCAS[30] to compute the g-values, crystal field parameters, wavefunction decomposition analysis, and transition magnetic moments of individual Dy(III) ions. Using the SINGLE_ANISO module, we computed the g-tensor associated with eight low-lying KDs for the three complexes. Using the SINGLE_ANISO code, we computed the CF parameters and constructed the ab initio blockade barrier by computing the transversal magnetic moment between each KDs to analyse the nature of magnetic relaxation.

The Cholesky decomposition for two-electron integrals was adapted to reduce the storage efficiency. The exchange spectrum (dipolar and exchange contributions), along with the magnetic properties of the dinuclear compound, was simulated using POLY_ANISO code based on obtained results from the ab initio calculations. The POLY_ANISO code has been successfully used to simulate the magnetic properties of highly anisotropic polynuclear complexes.[31-35]

Table S9. Calculated energy spectrum, g tensors, and the Φ and θ angles computed for complex **1**. Here Dy(1a) and Dy(1b) represent the two different Dy(III) sites present in complex **1**. The Φ and θ angles are described in Scheme 3.

Dy ions	**Kramers doublet**	**Energy (cm^{-1})**	**g_x**	**g_y**	**g_z**	**Φ (°)**	**θ (°)**
Dy(1a)	1	0.0	0.247	0.777	16.660	-	62.5
Dy(1b)	1	0.0	0.246	0.777	16.680		117.3

Dy(1a)	2	29.7	0.049	0.807	15.225	141.7	79.8
Dy(1b)	2	29.7	0.047	0.804	15.233	141.8	100.8
Dy(1a)	3	79.0	1.452	4.268	15.139	106.8	76.7
Dy(1b)	3	79.0	1.450	4.272	15.150	97.4	144.1
Dy(1a)	4	110.9	9.477	5.910	1.995	100.9	91.3
Dy(1b)	4	110.9	9.499	5.912	2.002	100.9	88.7
Dy(1a)	5	144.9	7.899	5.663	0.906	78.8	80.2
Dy(1b)	5	144.9	7.913	5.656	0.911	78.8	99.8
Dy(1a)	6	159.2	2.546	5.172	12.521	25.5	56.1
Dy(1b)	6	159.2	2.542	5.179	12.542	25.5	123.9
Dy(1a)	7	329.6	0.132	0.457	17.795	53.7	50.9
Dy(1b)	7	329.6	0.130	0.459	17.804	53.7	129.0
Dy(1a)	8	348.9	0.100	0.581	18.043	56.2	49.4
Dy(1b)	8	348.9	0.098	0.580	18.065	56.2	130.7

Table S10. Calculated energy spectrum, g tensors, and the Φ and θ angles computed for complex **2**. Here Dy(1a) and Dy(1b) represent the two different Dy(III) sites present in complex **2**. The Φ and θ angles are described in Scheme 3.

Dy ions	**Kramers doublet**	**Energy (cm^{-1})**	**g_x**	**g_y**	**g_z**	**Φ (°)**	**θ (°)**
Dy(1a)	1	0.0	0.489	1.446	18.366	-	111.9
Dy(1b)	1	0.0	0.489	1.444	18.333		68.1
Dy(1a)	2	42.8	3.031	4.587	11.362	29.2	102.2
Dy(1b)	2	42.8	3.024	4.586	11.340	29.2	77.9
Dy(1a)	3	75.7	2.400	4.597	10.759	68.1	168.1
Dy(1b)	3	75.7	2.402	4.587	10.762	68.1	12.0
Dy(1a)	4	110.6	0.418	1.779	13.564	91.9	155.3
Dy(1b)	4	110.6	0.416	1.770	13.564	91.8	24.6

Dy(1a)	5	131.0	0.820	1.280	12.126	87.4	154.9
Dy(1b)	5	131.0	0.811	1.280	12.123	87.4	25.1
Dy(1a)	6	200.3	0.131	0.209	16.445	57.8	67.6
Dy(1b)	6	200.3	0.131	0.208	16.416	57.9	112.5
Dy(1a)	7	301.6	0.001	0.087	19.048	106.2	135.0
Dy(1b)	7	301.6	0.001	0.086	19.047	106.1	45.0
Dy(1a)	8	367.2	0.018	0.067	19.387	74.0	129.7
Dy(1b)	8	367.2	0.018	0.067	19.368	73.9	50.3

Table S11. Calculated energy spectrum, g tensors, and the Φ and θ angles computed for complex **3**. Here Dy3(a) and Dy3(b) represent the two different Dy(III) sites present in complex **3**. The Φ and θ angles are described in Scheme 3.

Dy ions	Kramers doublet	Energy (cm^{-1})	g_x	g_y	g_z	Φ (°)	θ (°)
Dy(1a)	1	0.0	0.091	0.185	19.369	-	53.4
Dy(1b)	1	0.0	0.068	0.150	19.428		88.6
Dy(1a)	2	41.8	1.307	2.141	15.498	28.4	33.0
Dy(1b)	2	149.9	1.504	3.364	14.543	17.4	95.1
Dy(1a)	3	82.0	1.225	4.216	11.952	69.2	40.4
Dy(1b)	3	226.4	4.104	5.733	8.312	71.1	111.3
Dy(1a)	4	151.1	2.331	3.701	9.261	36.4	46.0
Dy(1b)	4	301.8	0.765	2.485	10.528	99.2	168.2
Dy(1a)	5	203.3	1.108	1.892	14.760	55.9	55.4
Dy(1b)	5	353.4	0.843	0.907	16.060	89.2	177.7
Dy(1a)	6	227.1	1.725	3.357	9.766	74.8	62.30
Dy(1b)	6	440.2	0.043	0.343	18.504	65.7	32.2
Dy(1a)	7	272.4	1.637	4.972	14.299	60.2	89.7
Dy(1b)	7	462.34	0.017	0.245	17.404	84.7	112.9

Dy(1a)	8	399.8	0.071	0.162	19.484	78.0	127.6
Dy(1b)	8	554.7	0.043	0.088	19.078	62.6	142.4

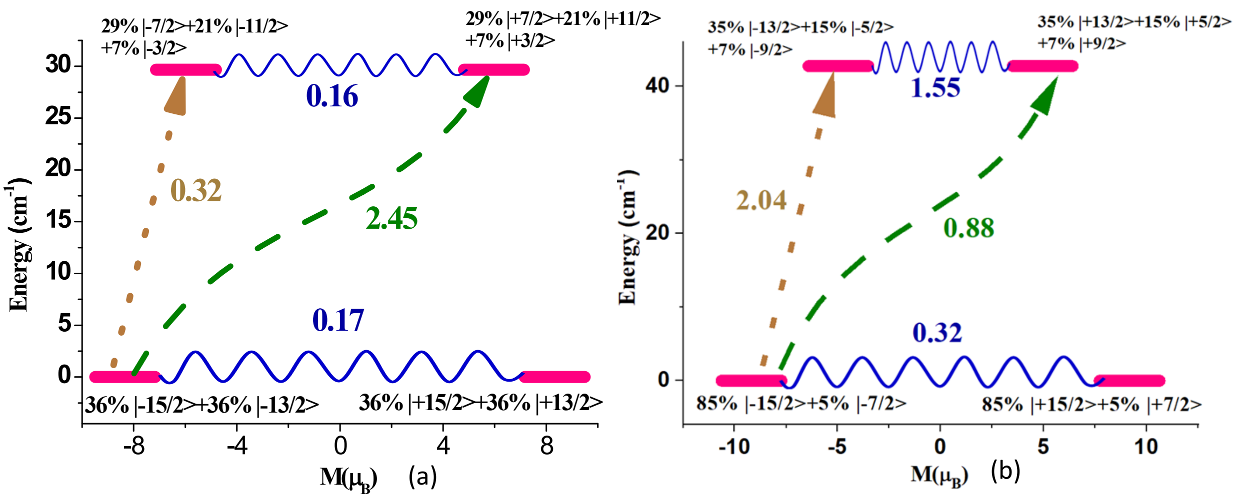

Figure S12. SINGLE_ANISO computed magnetization blockade barrier for a) complex **1** and b) **2**. Here we have shown only one relaxation for only one centre as Dy1(b)/Dy2(b) relaxes in similar pattern due to centrosymmetric environment.

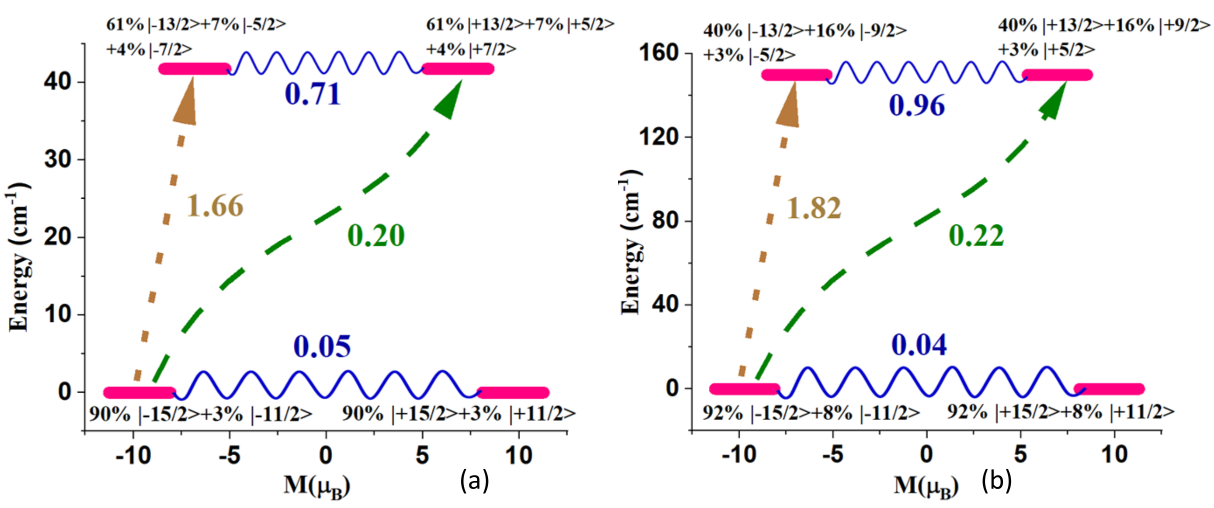

Figure S13. SINGLE_ANISO computed magnetization blockade barrier for a) Dy3(a) and b) Dy3(b) based mononuclear fragments of **3**.

Table S12. SINGLE_ANISO computed crystal field parameters for Dy^{III} in complex **1**.

k	q	B_k^q	B_k^q
		Dy1(a)	Dy1(b)
2	-2	2.42E-02	1.62E-02
	-1	**-2.50E+00**	**-2.51E+00**
	0	**-4.40E-01**	**-4.41E-01**
	1	-1.54E-01	-1.58E-01
	2	**1.79E+00**	**1.79E+00**
4	-4	-3.70E-05	-8.08E-05
	-3	-7.28E-02	-7.26E-02
	-2	1.05E-04	-2.11E-07
	-1	3.04E-02	3.05E-02
	0	-3.45E-03	-3.44E-03
	1	4.52E-03	4.65E-03
	2	1.32E-02	1.31E-02
	3	3.94E-03	3.40E-03
	4	-8.14E-03	-8.20E-03
6	-6	-1.54E-06	-2.36E-06
	-5	-1.24E-04	-1.19E-04
	-4	-3.57E-06	-4.58E-06
	-3	3.11E-05	3.43E-05
	-2	-9.76E-06	-9.00E-06
	-1	2.62E-04	2.62E-04
	0	2.46E-05	2.48E-05
	1	-6.28E-05	-6.36E-05
	2	-1.44E-04	-1.43E-04
	3	4.32E-05	3.96E-05
	4	-4.35E-05	-4.43E-05

	5	3.98E-05	3.70E-05
	6	-1.07E-05	-1.05E-05

Table S13. SINGLE_ANISO computed crystal field parameters for the Dy^{III} in complex **2**.

k	q	B_k^q	B_k^q
		Dy2(a)	Dy2(b)
2	-2	**5.93E-01**	**5.96E-01**
	-1	**-1.44E+00**	**-1.43E+00**
	0	**-1.09E+00**	**-1.09E+00**
	1	**2.46E-01**	**2.37E-01**
	2	**6.97E-01**	**6.86E-01**
4	-4	-1.27E-02	-1.28E-02
	-3	-5.13E-02	-5.07E-02
	-2	3.06E-03	3.10E-03
	-1	1.70E-02	1.72E-02
	0	-1.28E-03	-1.29E-03
	1	1.25E-02	1.23E-02
	2	6.65E-03	6.68E-03
	3	-1.85E-02	-1.84E-02
	4	-3.52E-02	-3.53E-02
6	-6	-2.07E-05	-2.03E-05
	-5	3.08E-04	3.12E-04
	-4	1.96E-04	1.97E-04
	-3	4.18E-04	4.12E-04
	-2	-2.77E-05	-2.88E-05
	-1	-1.17E-04	-1.17E-04
	0	-9.34E-07	-1.01E-06
	1	-1.42E-04	-1.45E-04
	2	-5.15E-06	-5.76E-06
	3	-8.84E-06	-1.85E-05
	4	-1.10E-04	-1.09E-04

	5	-1.68E-04	-1.86E-04
	6	5.89E-06	5.97E-06

Table S14. SINGLE_ANISO computed crystal field parameters for the Dy^{III} in complex **3**.

k	q	B_k^q	B_k^q
		Dy3(a)	Dy3(b)
2	-2	-8.08E-02	**-1.38E-01**
	-1	**1.29E+00**	**-7.26E-01**
	0	**-1.21E+00**	**-1.91E+00**
	1	**-1.05E+00**	**1.54E+00**
	2	**1.22E+00**	**2.53E+00**
4	-4	-1.34E-02	1.01E-02
	-3	4.17E-02	2.24E-03
	-2	-9.76E-03	4.73E-03
	-1	-9.08E-03	4.05E-03
	0	-2.98E-03	-4.88E-03
	1	-7.44E-04	-7.03E-03
	2	-1.30E-02	2.62E-02
	3	-3.33E-02	1.07E-02
	4	2.43E-02	-1.30E-02
6	-6	-2.52E-04	2.82E-04
	-5	6.11E-06	2.57E-04
	-4	1.83E-04	-1.79E-05
	-3	1.82E-04	-8.00E-06
	-2	-2.23E-05	-1.67E-04
	-1	-4.30E-05	5.05E-05
	0	2.07E-05	-3.59E-06
	1	7.86E-05	2.54E-05

	2	7.31E-05	1.47E-05
	3	1.06E-04	1.31E-04
	4	1.04E-04	1.59E-04
	5	-4.08E-04	-8.79E-05
	6	6.03E-05	2.37E-04

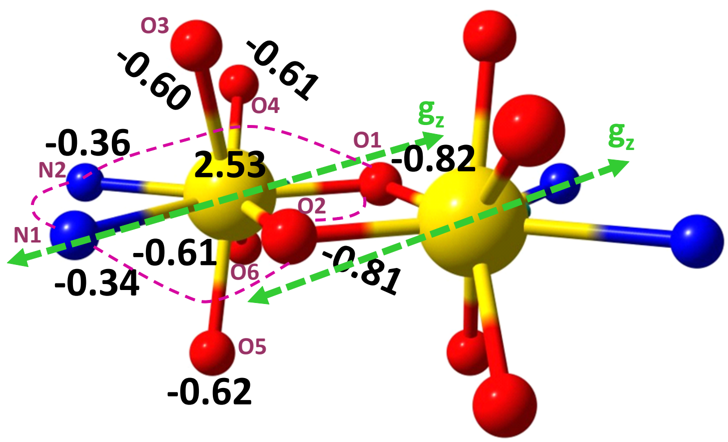

Figure S14. CASSCF computed LoProp charges on the Dy and first coordination sphere ligated atoms in complex **1**.

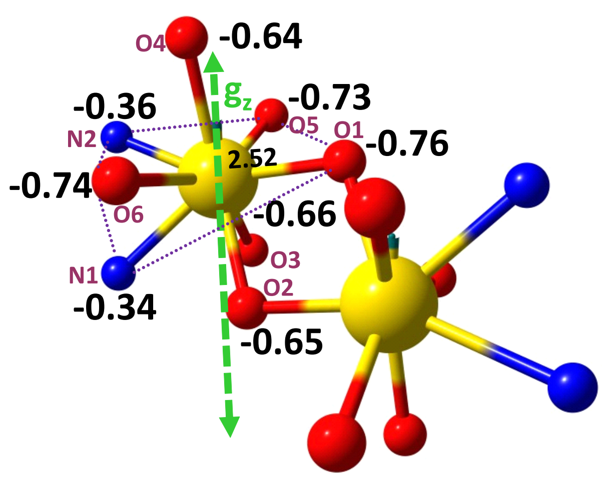

Figure S15. CASSCF computed LoProp charges on the Dy and first coordination sphere ligated atoms in complex **2**.

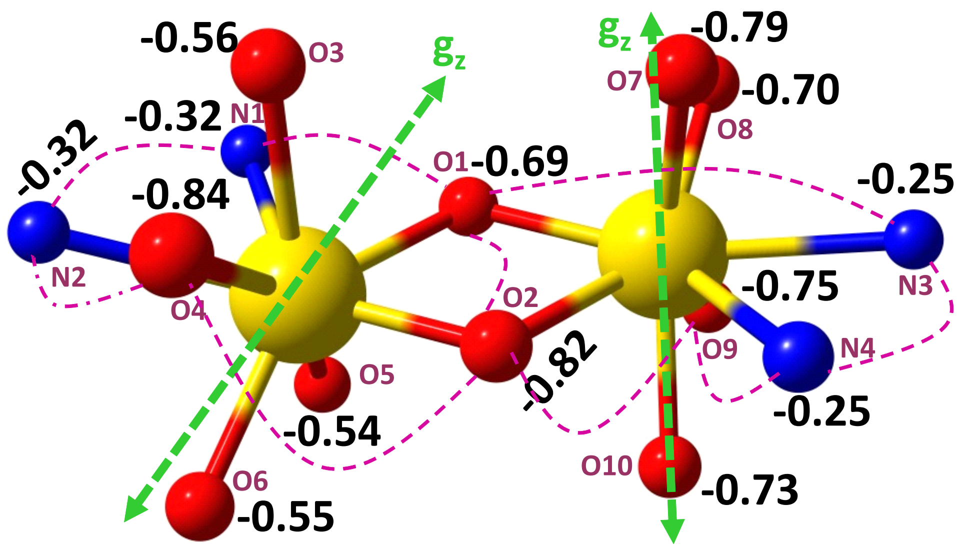

Figure S16. CASSCF computed LoProp charges on the Dy and first coordination sphere ligated atoms in complex **3**.

Table S15. CASSCF computed LoProp charges per central atom and first coordination sphere ligand atoms in the ground state of complexes **1-3**.

	Atoms	**1**	Atoms	**2**	Atoms	**3**	Atoms	**3**
	Dy(1a)/Dy(1b)	2.53	Dy(1a)/Dy(1b)	2.52	Dy(1a)		Dy(1b)	
	O3	-0.60	O1	-0.76	O3	-0.56	O1	-0.78
	O4	-0.61	O5	-0.73	O6	-0.55	O2	-0.81
Hard Plane atoms	O5	-0.62	N2	-0.36	O5	-0.54	O9	-0.75
	O6	-0.61	O6	-0.74			N4	-0.25
			N1	-0.34			N3	-0.25
Average		-0.61		-0.58		-0.55		-0.57
Axial	O1	-0.82	O4	-0.64	O1	-0.69	O7	-0.79

coordination atoms	O2	-0.81	O3	-0.66	O2	-0.82	O8	-0.70
	N1	-0.34	O2	-0.65	N2	-0.32	O10	-0.73
	N2	-0.36			O4	-0.84		
					N1	-0.32		
Average		-0.58		-0.65		-0.60		-0.74

Table S16. SINGLE_ANISO computed wave function decomposition analysis for Dy1 and Dy2 centres in complex **1**. The major dominating values are kept in bold.

±*mJ*	*wave function decomposition analysis* **Dy@1**
KD1	**37.63% |±13/2⟩ + 37.08% |±15/2⟩** + 16.29% |±9/2⟩
KD2	**30.65% |±7/2⟩** + 21.97% |±11/2⟩ + 16.97% |±15/2⟩ + 12.08% |±9/2⟩
KD3	**48.33% |±1/2⟩** + 19.68% |±3/2⟩ + 16.06% |±5/2⟩
KD4	**23.45% |±3/2⟩ +** 22.15% |±1/2⟩ + 15.25% |±15/2⟩ + 12.57% |±5/2⟩ + 10.08% |±11/2⟩
KD5	**33.49% |±3/2⟩**+ 20.05% |±13/2⟩ + 12.74% |±5/2⟩
KD6	**23.95% |±13/2⟩** + 19.26% |±15/2⟩ + 18.06% |±1/2⟩ + 16.96% |±11/2⟩ + 14.80% |±5/2⟩
KD7	**34.27% |±7/2⟩**+ 23.17% |±11/2⟩ + 18.17% |±5/2⟩ + 14.21% |±9/2⟩
KD8	**41.39% |±9/2⟩**+ 22.09% |±7/2⟩ + 13.74% |±5/2⟩
±*mJ*	*wave function decomposition analysis* **Dy@2**
KD1	**38.00% |±13/2⟩ + 36.78% |±15/2⟩** + 16.15% |±9/2⟩
KD2	**30.61% |±7/2⟩** + 21.93% |±11/2⟩ + 16.99% |±15/2⟩ + 12.14% |±9/2⟩
KD3	**48.20% |±1/2⟩** + 19.78% |±3/2⟩ + 16.07% |±5/2⟩
KD4	**23.16% |±3/2⟩ +** 22.40% |±1/2⟩ + 15.39% |±15/2⟩ + 12.58% |±5/2⟩ + 10.02% |±11/2⟩
KD5	**33.72% |±3/2⟩**+ 20.06% |±13/2⟩ + 12.56% |±5/2⟩
KD6	**23.65% |±13/2⟩** + 19.36% |±15/2⟩ + 18.02% |±1/2⟩ + 17.13% |±11/2⟩ + 14.88% |±5/2⟩
KD7	**34.08% |±7/2⟩**+ 23.24% |±11/2⟩ + 18.33% |±5/2⟩ + 14.21% |±9/2⟩
KD8	**41.41% |±9/2⟩**+ 22.36% |±7/2⟩ + 13.67% |±5/2⟩

Table S17. SINGLE_ANISO computed wave function decomposition analysis for Dy1 centre and Dy2 centre in complex **2**. The major dominating values are kept in bold.

±*mJ*	*wave function decomposition analysis* **Dy@1**
KD1	**84.47%|±15/2⟩** + 6.25% |±7/2⟩
KD2	**46.20% |±13/2⟩** + 18.41% |±5/2⟩ + 10.51% |±9/2⟩
KD3	**24.46% |±11/2⟩** + 17.35% |±13/2⟩ + 15.52% |±7/2⟩ + 13.02% |±3/2⟩
KD4	**28.26% |±1/2⟩ +** 16.84% |±9/2⟩ + 16.07% |±11/2⟩ + 14.16% |±5/2⟩ + 10.74% |±3/2⟩
KD5	**19.56% |±7/2⟩**+ 18.83% |±9/2⟩ + 18.21% |±3/2⟩ + 12.74% |±13/2⟩ + 11.64% |±11/2⟩ + 10.67% |±1/2⟩
KD6	**27.48% |±11/2⟩** + 18.90% |±9/2⟩ + 16.65% |±13/2⟩ + 13.03% |±7/2⟩ + 12.87% |±5/2⟩
KD7	**27.44% |±1/2⟩**+ 18.18% |±3/2⟩ + 17.17% |±7/2⟩ + 15.28% |±5/2⟩ + 14.31% |±5/2⟩
KD8	**25.70% |±5/2⟩**+ 25.65% |±3/2⟩ + 17.41% |±7/2⟩ + 17.33% |±1/2⟩
±*mJ*	*wave function decomposition analysis* **Dy@2**
KD1	**84.47%|±15/2⟩** + 6.26% |±7/2⟩
KD2	**46.16% |±13/2⟩** + 18.40% |±5/2⟩ + 10.46% |±9/2⟩
KD3	**24.33% |±11/2⟩** + 17.33% |±13/2⟩ + 15.53% |±7/2⟩ + 12.91% |±3/2⟩
KD4	**28.31% |±1/2⟩ +** 16.94% |±9/2⟩ + 16.02% |±11/2⟩ + 14.15% |±5/2⟩ + 10.70% |±3/2⟩
KD5	**19.64% |±7/2⟩**+ 18.78% |±9/2⟩ + 18.35% |±3/2⟩ + 12.83% |±13/2⟩ + 11.58% |±11/2⟩ + 10.52% |±1/2⟩
KD6	**27.60% |±11/2⟩** + 18.79% |±9/2⟩ + 16.65% |±13/2⟩ + 13.05% |±7/2⟩ + 12.87% |±5/2⟩
KD7	**27.70% |±1/2⟩**+ 18.07% |±3/2⟩ + 17.05% |±7/2⟩ + 15.14% |±5/2⟩ + 14.34% |±5/2⟩
KD8	**25.79% |±5/2⟩**+ 25.68% |±3/2⟩ + 17.47% |±7/2⟩ + 17.14% |±1/2⟩

Table S18. SINGLE_ANISO computed wave function decomposition analysis for Dy1 centre and Dy2 centre in complex **3**. The major dominating values are kept in bold.

±mJ	*wave function decomposition analysis* **Dy@1**
KD1	**91.73%|±15/2⟩** + 3.35% |±11/2⟩
KD2	**66.13% |±13/2⟩** + 10.69% |±5/2⟩
KD3	**29.23% |±1/2⟩** + 27.51% |±3/2⟩ + 15.27% |±13/2⟩ + 10.99% |±11/2⟩
KD4	**40.82% |±11/2⟩ +** 24.13% |±1/2⟩
KD5	**24.09% |±9/2⟩**+ 16.98% |±11/2⟩ + 15.14% |±5/2⟩ + 14.82% |±3/2⟩ + 12.52% |±7/2⟩
KD6	**22.18% |±3/2⟩** + 19.45% |±7/2⟩ + 18.20% |±9/2⟩ + 16.49% |±5/2⟩ + 10.07% |±11/2⟩
KD7	**31.09% |±7/2⟩**+ 26.69% |±9/2⟩ + 23.87% |±5/2⟩
KD8	**22.03% |±1/2⟩**+ 21.05% |±3/2⟩ + 19.96% |±5/2⟩ + 19.42% |±7/2⟩ + 12.20% |±9/2⟩
±mJ	*wave function decomposition analysis* **Dy@2**
KD1	**91.28%|±15/2⟩** + 8.14% |±11/2⟩
KD2	**60.90% |±13/2⟩** + 24.94% |±9/2⟩
KD3	**29.90% |±7/2⟩** + 18.37% |±11/2⟩ + 14.99% |±13/2⟩ + 12.80% |±3/2⟩ + 10.56% |±5/2⟩ + 10.15% |±3/2⟩
KD4	**27.68% |±5/2⟩ +** 27.13% |±11/2⟩ **+** 12.65% |±3/2⟩
KD5	**37.44% |±1/2⟩**+ 23.21% |±3/2⟩ + 12.93% |±9/2⟩ + 11.11% |±11/2⟩
KD6	**20.84% |±9/2⟩** + 19.67% |±7/2⟩ + 18.64% |±5/2⟩ + 14.44% |±3/2⟩ + 14.42% |±11/2⟩
KD7	**36.18% |±1/2⟩**+ 26.68% |±3/2⟩ + 10.76% |±5/2⟩ + 10.51% |±9/2⟩
KD8	**28.29% |±7/2⟩**+ 22.81% |±9/2⟩ + 20.80% |±5/2⟩ + 12.83% |±11/2⟩

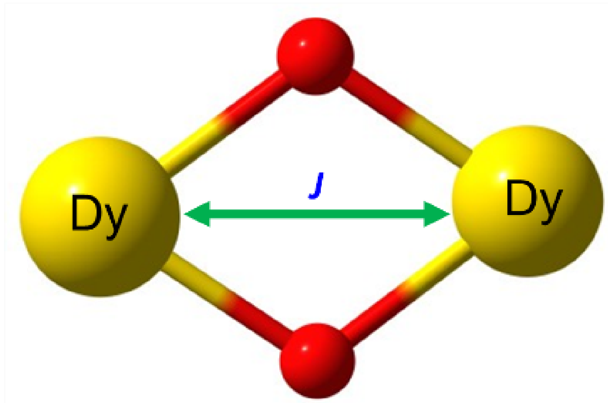

Scheme S1. Exchange model employed model Dy-Dy series (**1-3**)

$$\hat{H}_{exch} = -J\hat{S}_{Dy}\hat{S}_{Dy}$$

The foregoing exchange matrix has been written on the basis of lowest spin-orbit multiplets on magnetic centres.

Table S19. BS-DFT computed energies of high-spin and broken-symmetry solution of complex M**1** using H = $-2JS_1S_2$ formalism.

Solution	**Energy (Eh)**	ρ^{Gd1}	ρ^{Gd2}	<S**2>	**J** (cm^{-1})	**J** value Rescaled to Dy^{III} spin (= **J**x25/49)
HS	-27593.884613148628	7.01	7.01	56.0109	−0.68	**-0.34**
BS1	-27593.884681936219	7.01	−7.01	7.0119		

J values are estimated using the following equation,

$$\boldsymbol{J} = -\frac{E_{HS} - E_{BS}}{s_{HS}^{2} - s_{BS}^{2}}$$

Table S20. BS-DFT computed energies of high-spin and broken-symmetry solution of complex M2 using H=-$2JS_1S_2$ formalism.

Solution	**Energy (Eh)**	ρ^{Gd1}	ρ^{Gd2}	**<S**2>**	**J** (cm^{-1})	**J** value Rescaled to Dy^{III} spin (= **J**x25/49)
HS	-26403.516547281051	7.01	7.01	56.0109	-0.66	**-0.33**
BS1	-26403.516611767995	7.01	−7.01	7.0119		

J values are estimated using the following equation,

$$\boldsymbol{J} = -\frac{E_{HS} - E_{BS}}{s_{HS}^{2} - s_{BS}^{2}}$$

Table S21. BS-DFT computed energies of high-spin and broken-symmetry solution of complex M3 using H=-$2JS_1S_2$ formalism.

Solution	**Energy (Eh)**	ρ^{Gd1}	ρ^{Gd2}	**<S**2>**	**J** (cm^{-1})	**J** value Rescaled to Dy^{III} spin (= **J**x25/49)
HS	-25854.682010876866	7.01	7.01	56.0120	-0.20	**-0.10**
BS1	-25854.682033786190	7.01	−7.01	7.0121		

J values are estimated using the following equation,

$$J = -\frac{E_{HS} - E_{BS}}{S_{HS}^{2} - S_{BS}^{2}}$$

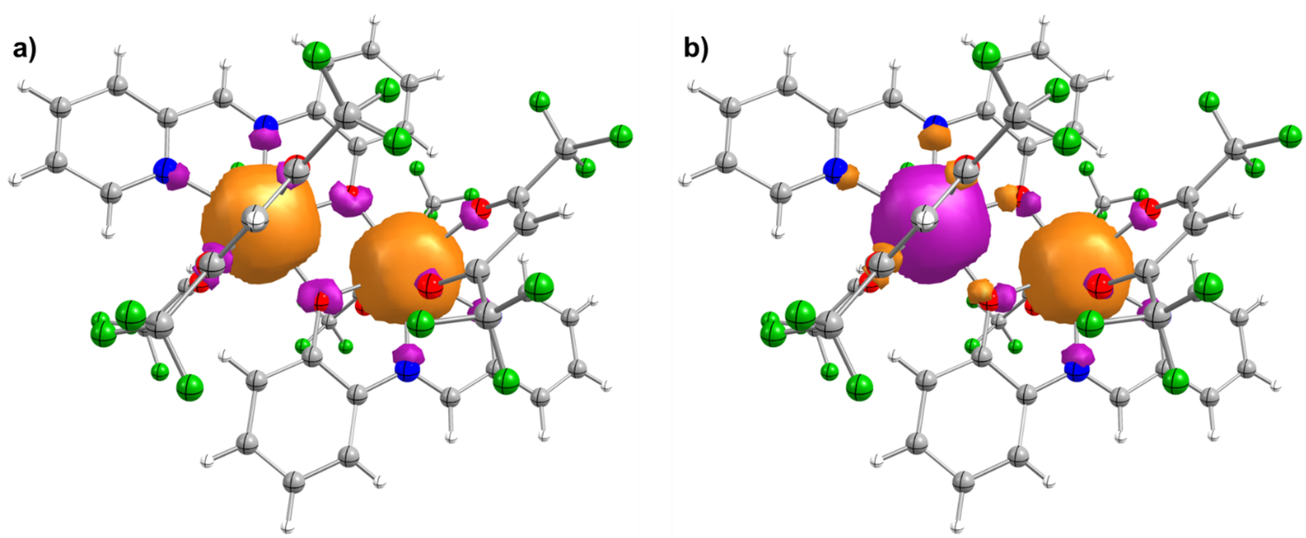

Figure S17. DFT calculated spin-density plot for the ground state (S=0) of complex M1 (a) HS and (b) BS; the positive and negative spin densities are represented by orange and purple colour, respectively. The isodensity surface represented here corresponds to a value of 0.001 e^{-}/ $bohr^3$.

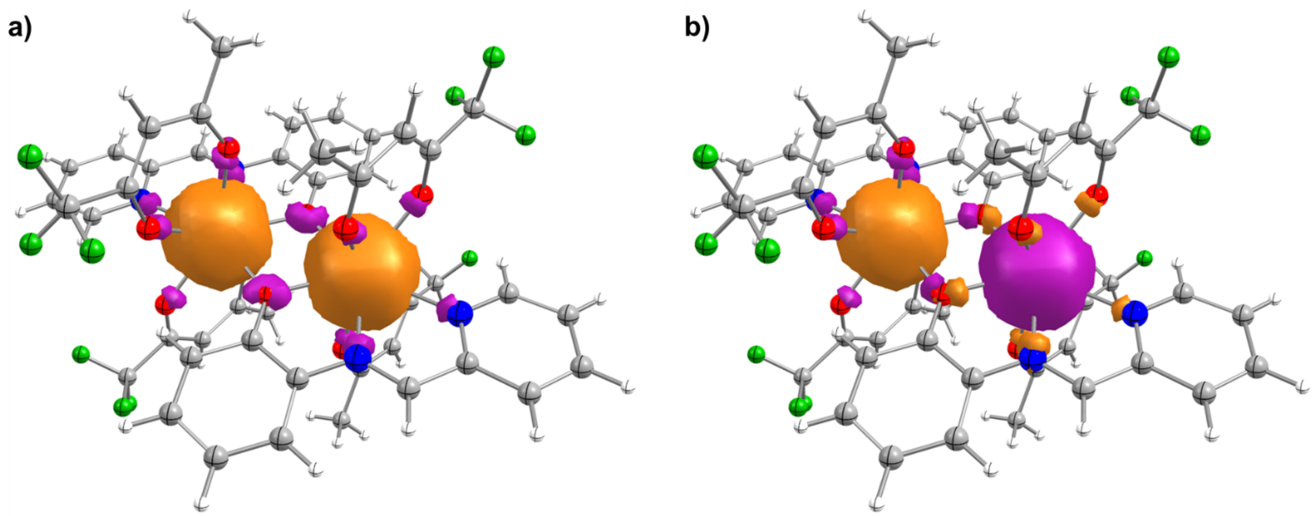

Figure S18. DFT calculated spin-density plot for the ground state (S=0) of complex M2 (a) HS and (b) BS; the positive and negative spin densities are represented by orange and purple colour, respectively. The isodensity surface represented here corresponds to a value of 0.001 e⁻/ bohr^3.

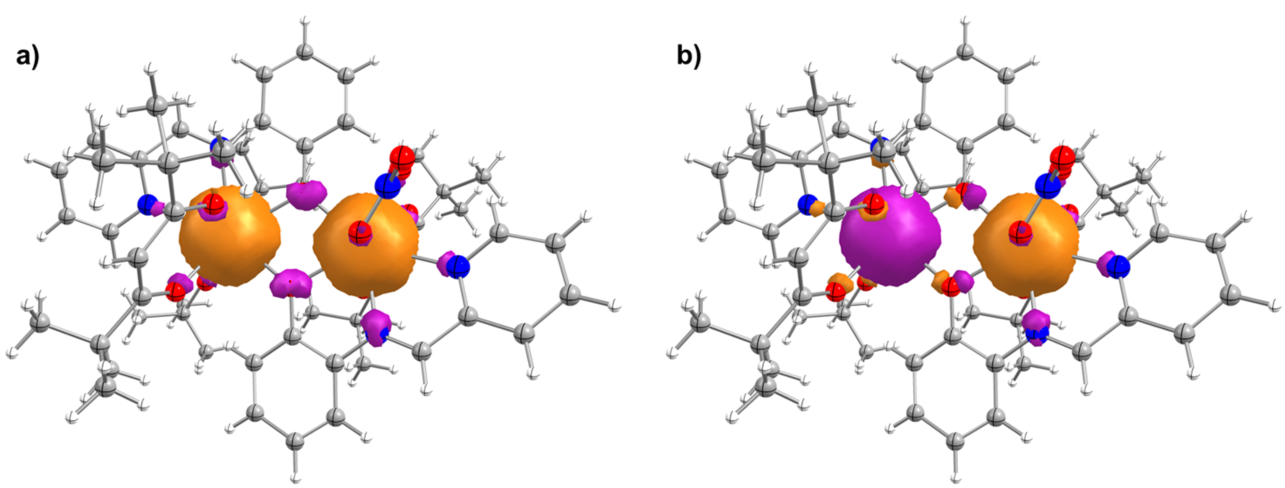

Figure S19. DFT calculated spin-density plot for the ground state (S = 0) of complex M3 (a) HS and (b) BS; the positive and negative spin densities are represented by orange and purple colour, respectively. The isodensity surface represented here corresponds to a value of 0.001 e^{-}/ $bohr^3$.

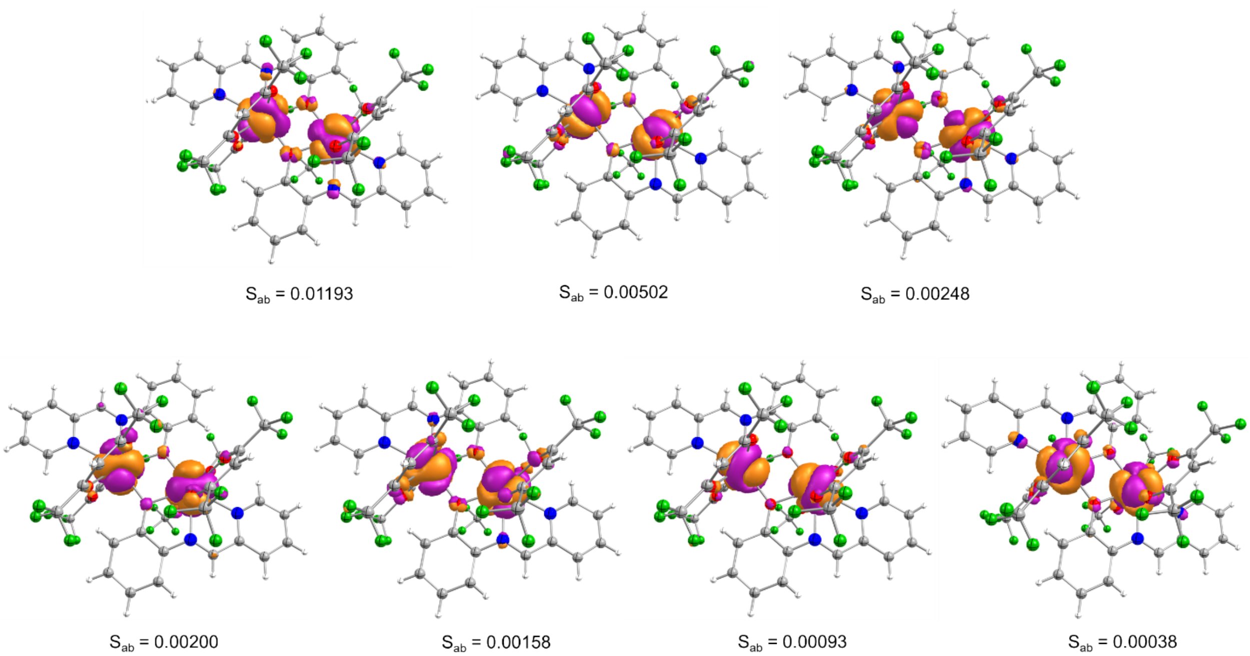

Figure S20. DFT calculated overlap integrals for complex M1. The isodensity surface represented here corresponds to a value of 0.03 e^{-}/ $bohr^3$.

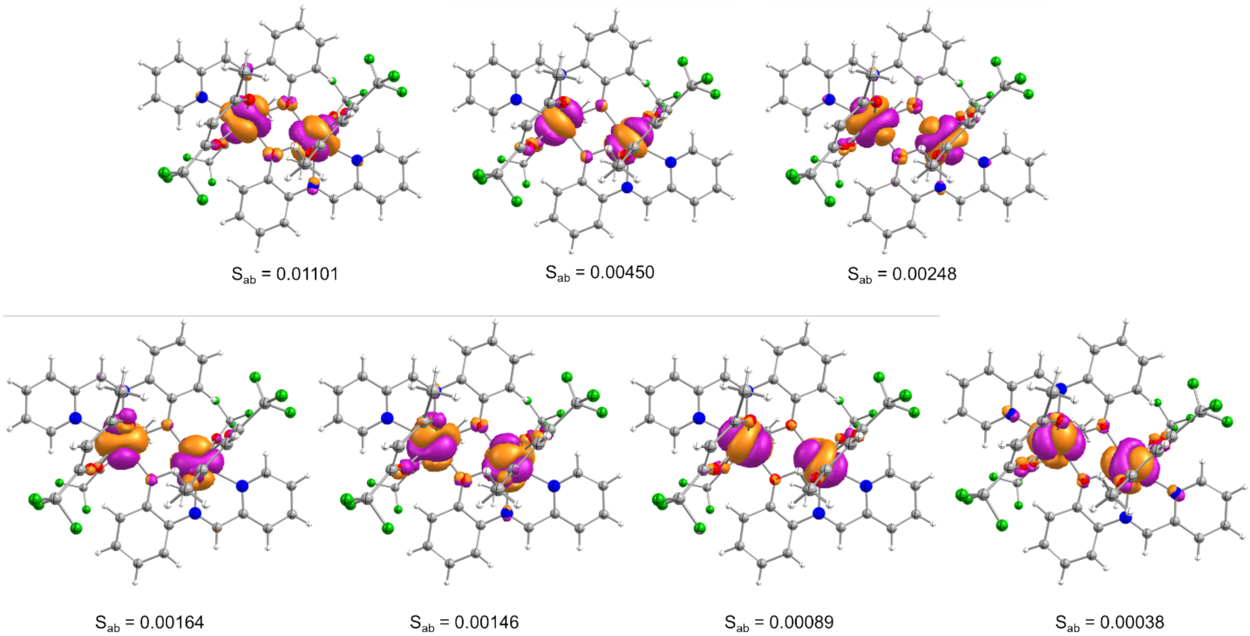

Figure S21. DFT calculated overlap integrals for complex M2. The isodensity surface represented here corresponds to a value of 0.03 e^{-}/ $bohr^3$.

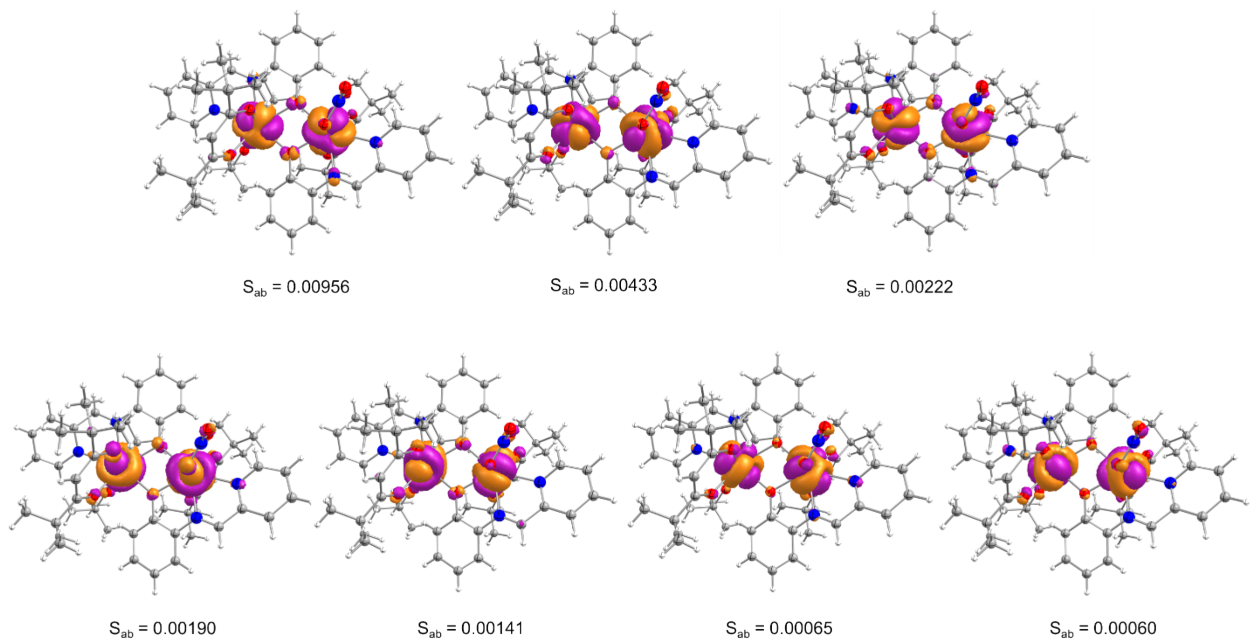

Figure S22. DFT calculated overlap integrals for complex M3. The isodensity surface represented here corresponds to a value of 0.03 e^{-}/ $bohr^3$.

Table S22. Energies (cm^{-1}), corresponding tunnel splitting (Δ_{tun}) and g tensors of the low-lying exchange doublet state in complex **1-3**.

Complex **1**					
Energy of Exchange Doublet	Δ_{tun}/cm^{-1}	g_z	Energy	Δ_{tun}/cm^{-1}	g_z
0.0000 0.0006	0.0006	0.024	31.87569 31.89325	0.017	30.143
2.1756 2.1758	0.002	33.401	31.9820 31.9957	0.013	130.138
29.5114 29.5302	0.018	0.068	59.3038 59.3110	0.007	0.010
29.6859 29.6996	0.013	0.069	61.5901 61.5969	0.006	30.565
Complex **2**					
Energy	Δ_{tun}/cm^{-1}	g_z	Energy	Δ_{tun}/cm^{-1}	g_z
0.0000 0.0009	0.0009	0.035	43.7937 43.8910	0.097	28.280
1.5238		36.645	44.1717	0.050	28.393

1.5287	0.0049		44.2223		
42.8184 42.8522	0.033	0.104	85.9314 85.9332	0.002	0.027
43.2314 43.3072	0.075	0.156	86.5907 86.7626	0.2	22.600
Complex **3**					
Energy	Δ_{tun}/cm^{-1}	g_{zz}	Energy	Δ_{tun}/cm^{-1}	g_z
0.0000 0.0002	0.0002	16.002	150.1008 150.1051	0.0043	11.168
2.1699 2.1702	0.0003	35.241	151.8862 151.8918	0.0056	32.336
42.1553 42.1573	0.0020	17.197	192.2602 192.3089	0.048	13.054
43.5862 43.5991	0.0129	30.564	193.2379 193.3074	0.069	26.667

Table S23. Crystal data and structure refinement details of 1 to 3.

	1	**2**	**3**
Empirical formula	$C_{44}H_{22}Dy_2F_{24}N_4O_{10}$	$C_{44}H_{28}Dy_2F_{12}N_4O_{10}$	$C_{57}H_{75}Dy_2N_5O_{11}$
Formula weight	1547.65	1325.70	1331.22
Temperature/K	293(2)	150.0	150.01
Crystal system	monoclinic	monoclinic	monoclinic
Space group	$P2_1/n$	$P2_1/n$	$P2_1/n$
a/Å	10.8075(3)	10.559(3)	13.2636(18)
b/Å	17.3606(5)	17.123(3)	35.219(5)
c/Å	13.7617(4)	12.969(2)	13.709(2)
α/°	90	90	90

β/°	90.7690(10)	91.215(14)	97.401(3)
γ/°	90	90	90
Volume/Å^3	2581.80(13)	2344.3(9)	6350.7(16)
Z	2	2	4
ρ_{calc}g/cm^3	1.991	1.878	1.392
μ/mm^{-1}	3.018	3.271	2.391
F(000)	1484.0	1280.0	2688.0
Crystal size/mm^3	0.056 × 0.033 × 0.027	0.091 × 0.078 × 0.057	0.046 × 0.037 × 0.024
Radiation	MoKα (λ = 0.71073)	MoKα (λ = 0.71073)	MoKα (λ = 0.71073)
2Θ range for data collection/°	4.824 to 56.72	5.028 to 50.736	4.584 to 50.998
Index ranges	$-11 \leq h \leq 14$, $-23 \leq k \leq 23$, $-18 \leq l \leq 18$	$-12 \leq h \leq 12$, $-20 \leq k \leq 20$, $-15 \leq l \leq 15$	$-16 \leq h \leq 16$, $-40 \leq k \leq 42$, $-16 \leq l \leq 16$
Reflections collected	27196	21676	57708
Independent reflections	6447 [R_{int} = 0.0251, R_{sigma} = 0.0208]	4227 [R_{int} = 0.0212, R_{sigma} = 0.0158]	11811 [R_{int} = 0.0423, R_{sigma} = 0.0322]
Data/restraints/ parameters	6447/0/379	4227/6/342	11811/0/676
Goodness-of-fit on F^2	1.035	1.171	1.246

Final R indexes [I>=2σ (I)]	R_1 = 0.0358, wR_2 = 0.0964	R_1 = 0.0290, wR_2 = 0.0659	R_1 = 0.0584, wR_2 = 0.1287
Final R indexes [all data]	R_1 = 0.0441, wR_2 = 0.1035	R_1 = 0.0291, wR_2 = 0.0660	R_1 = 0.0621, wR_2 = 0.1310

References

1. J. Long, F. Habib, P.-H. Lin, I. Korobkov, G. Enright, L. Ungur, W. Wernsdorfer, L. F. Chibotaru and M. Murugesu, Single-molecule magnet behavior for an antiferromagnetically superexchange-coupled dinuclear dysprosium (III) complex, *J. Am. Chem. Soc.*, 2011, **133**, 5319-5328.
2. W.-M. Wang, S.-Y. Wang, H.-X. Zhang, H.-Y. Shen, J.-Y. Zou, H.-L. Gao, J.-Z. Cui and B. Zhao, Modulating single-molecule magnet behaviour of phenoxo-O bridged lanthanide (III) dinuclear complexes by using different β-diketonate coligands, *Inorg. Chem. Front.*, 2016, **3**, 133-141.
3. L. Zhao, J. Wu, H. Ke and J. Tang, Three dinuclear lanthanide (iii) compounds of a polydentate Schiff base ligand: Slow magnetic relaxation behaviour of the Dy III derivative, *CrystEngComm*, 2013, **15**, 5301-5306.
4. S. Yu, Z. Hu, Z. Chen, B. Li, Y.-Q. Zhang, Y. Liang, D. Liu, D. Yao and F. Liang, Two dy (III) single-molecule magnets with their performance tuned by schiff base ligands, *Inorg. Chem.*, 2019, **58**, 1191-1200.

5. K. Zhang, D. Liu, V. Vieru, L. Hou, B. Cui, F.-S. Guo, L. F. Chibotaru and Y.-Y. Wang, Transitions of two magnetic interaction states in dinuclear Dy (III) complexes via subtle structural variations, *Dalton Trans.*, 2017, **46**, 638-642.

6. Y.-N. Guo, X.-H. Chen, S. Xue and J. Tang, Modulating magnetic dynamics of three Dy2 complexes through keto–enol tautomerism of the o-vanillin picolinoylhydrazone ligand, *Inorg. Chem.*, 2011, **50**, 9705-9713.

7. A.-J. Hutchings, F. Habib, R. J. Holmberg, I. Korobkov and M. Murugesu, Structural rearrangement through lanthanide contraction in dinuclear complexes, *Inorg. Chem.*, 2014, **53**, 2102-2112.

8. S. Biswas, S. Das, G. Rogez and V. Chandrasekhar, Hydrazone-Ligand-Based Homodinuclear Lanthanide Complexes: Synthesis, Structure, and Magnetism, *Eur. J. Inorg. Chem.*, 2016, **2016**, 3322-3329.

9. S.-Y. Lin, G.-F. Xu, L. Zhao, Y.-N. Guo, Y. Guo and J. Tang, Observation of slow magnetic relaxation in triple-stranded lanthanide helicates, *Dalton Trans.*, 2011, **40**, 8213-8217.

10. Y.-J. Wang, D.-F. Wu, J. Gou, Y.-Y. Duan, L. Li, H.-H. Chen, H.-L. Gao and J.-Z. Cui, Modulation of the properties of dinuclear lanthanide complexes through utilizing different β-diketonate co-ligands: near-infrared luminescence and magnetization dynamics, *Dalton Trans.*, 2020, **49**, 2850-2861.

11. Y. Ge, Y. Huang, J. L. B. Montenegro, Y. Cui, W. Liu, Y. Li and B. L. Wang, Synthesis, Structures, and Single-Molecule Magnetic Properties of Three Dy2 Complexes, *Chem. Asian J.*, 2019, **14**, 986-994.

12. H. Tian, L. Ungur, L. Zhao, S. Ding, J. Tang and L. F. Chibotaru, Exchange Interactions Switch Tunneling: A Comparative Experimental and Theoretical Study on Relaxation Dynamics by Targeted Metal Ion Replacement, *Chem. Eur. J.*, 2018, **24**, 9928-9939.

13. Y.-X. Chang, W.-M. Wang, R.-X. Zhang, H.-Y. Shen, X.-P. Zhou, N.-N. Wang, J.-Z. Cui and H.-L. Gao, Dinuclear Ln (III) complexes constructed from an 8-hydroxyquinoline Schiff base derivative with different terminal groups show differing slow magnetic relaxation, *New J Chem*, 2017, **41**, 6251-6261.

14. J. Acharya, N. Ahmed, J. F. Gonzalez, P. Kumar, O. Cador, S. K. Singh, F. Pointillart and V. Chandrasekhar, Slow magnetic relaxation in a homo dinuclear Dy (III) complex in a pentagonal bipyramidal geometry, *Dalton Trans..* 2020, **49**, 13110-13122.

15. S. Xue, Y. N. Guo, L. Ungur, J. Tang and L. F. Chibotaru, Tuning the Magnetic Interactions and Relaxation Dynamics of Dy2 Single-Molecule Magnets, *Eur. J. Chem*, 2015, **21**, 14099-14106.

16. H.-M. Dong, H.-Y. Li, Y.-Q. Zhang, E.-C. Yang and X.-J. Zhao, Magnetic relaxation dynamics of a centrosymmetric Dy2 single-molecule magnet triggered by magnetic-site dilution and external magnetic field, *Inorg. Chem.*, 2017, **56**, 5611-5622.

17. J.-Y. Ge, H.-Y. Wang, J. Su, J. Li, B.-L. Wang, Y.-Q. Zhang and J.-L. Zuo, Modulating the magnetic interaction in new triple-decker dysprosium (III) single-molecule magnets, *Inorg. Chem.*, 2018, **57**, 1408-1416.

18. D. Li, M.-M. Ding, Y. Huang, D. F. T. Yepes, H. Li, Y. Li, Y.-Q. Zhang and J. Yao, Evolution from a single relaxation process to two-step relaxation processes of Dy 2 single-molecule magnets via the modulations of the terminal solvent ligands, *Dalton Trans..* 2021, **50**, 217-228.

19. Y. Ge, D. Li, G. Wang, Y. Cui, M. S. Najib, Y. Li and B. L. Wang, Single-Molecule Magnetism in Three Dy2 Complexes from the Use of a Pentadentate Schiff Base Ligand and Different Benzoates, *Chem. Asian J.*, 2019, **14**, 2846-2852.

20. W. Zhang, S.-M. Xu, Z.-X. Zhu, J. Ru, Y.-Q. Zhang and M.-X. Yao, Strong intramolecular Dy III–Dy III magnetic couplings up to 15.00 cm− 1 in phenoxyl-bridged dinuclear 4f complexes, *New J. Chem.*. 2020, **44**, 2083-2090.

21. W.-Y. Zhang, Y.-M. Tian, H.-F. Li, P. Chen, W.-B. Sun, Y.-Q. Zhang and P.-F. Yan, A series of dinuclear Dy (III) complexes bridged by 2-methyl-8-hydroxylquinoline: replacement on the periphery coordinated β-diketonate terminal leads to different single-molecule magnetic properties, *Dalton Trans.*. 2016, **45**, 3863-3873.

22. W.-Y. Zhang, Y.-Q. Zhang, S.-D. Jiang, W.-B. Sun, H.-F. Li, B.-W. Wang, P. Chen, P.-F. Yan and S. Gao, Dramatic impact of the lattice solvent on the dynamic magnetic relaxation of dinuclear dysprosium single-molecule magnets, *Inorg. Chem. Front.*, 2018, **5**, 1575-1586.

23. F. Aquilante, J. Autschbach, R. K. Carlson, L. F. Chibotaru, M. G. Delcey, L. De Vico, I. Fdez. Galván, N. Ferré, L. M. Frutos and L. Gagliardi, Molcas 8: New capabilities for multiconfigurational quantum chemical calculations across the periodic table.*Journal*, 2016.

24. P.-Å. Malmqvist and B. O. Roos, The CASSCF state interaction method, *Chemical physics letters*, 1989, **155**, 189-194.

25. P. A. M. J. Finley, B. O Roos, L. Serrano-Andres, , The multi-state CASPT2 method, *Chem. Phys. Lett*, 1998, **288**, 9-306.

26. P. Å. Malmqvist, K. Pierloot, A. R. M. Shahi, C. J. Cramer and L. Gagliardi, The restricted active space followed by second-order perturbation theory method: Theory and application to the study of Cu O 2 and Cu 2 O 2 systems, *J. Chem. Phys.* , 2008, **128**, 204109.

27. P. Å. Malmqvist, A. Rendell and B. O. Roos, The restricted active space self-consistent-field method, implemented with a split graph unitary group approach, *J. Phys. Chem.* , 1990, **94**, 5477-5482.

28. D. Ma, G. Li Manni and L. Gagliardi, The generalized active space concept in multiconfigurational self-consistent field methods, *J.Chem. Phys.* , 2011, **135**, 044128.

29. B. O. Roos, V. Veryazov and P.-O. Widmark, Relativistic atomic natural orbital type basis sets for the alkaline and alkaline-earth atoms applied to the ground-state potentials for the corresponding dimers, *Chem. Acc*, 2004, **111**, 345-351.

30. P. Å. Malmqvist, B. O. Roos and B. Schimmelpfennig, The restricted active space (RAS) state interaction approach with spin–orbit coupling, *Chem. Phys. Lett.* , 2002, **357**, 230-240.

31. K. L. Harriman, J. J. Le Roy, L. Ungur, R. J. Holmberg, I. Korobkov and M. Murugesu, Cycloheptatrienyl trianion: an elusive bridge in the search of exchange coupled dinuclear organolanthanide single-molecule magnets, *Chem. Sci.* , 2017, **8**, 231-240.

32. P. Zhang, M. Perfetti, M. Kern, P. P. Hallmen, L. Ungur, S. Lenz, M. R. Ringenberg, W. Frey, H. Stoll and G. Rauhut, Exchange coupling and single molecule magnetism in redox-active tetraoxolene-bridged dilanthanide complexes, *Chem. Sci.* , 2018, **9**, 1221-1230.

33. I. F. Diaz-Ortega, J. M. Herrera, D. Aravena, E. Ruiz, T. Gupta, G. Rajaraman, H. Nojiri and E. Colacio, Designing a Dy2 single-molecule magnet with two well-differentiated relaxation processes by using a nonsymmetric Bis-bidentate bipyrimidine-n-oxide ligand: a comparison with mononuclear counterparts, *Inorg. Chem.* , 2018, **57**, 6362-6375.

34. I. F. Díaz-Ortega, J. M. Herrera, Á. Reyes Carmona, J. R. Galán-Mascarós, S. Dey, H. Nojiri, G. Rajaraman and E. Colacio, A Chiral Bipyrimidine-Bridged Dy2 SMM: A Comparative Experimental and Theoretical study of the Correlation between the Distortion of the DyO6N2 coordination sphere and the anisotropy barrier, *Front. Chem*, 2018, 537.

35. H.-M. Dong, H.-Y. Li, Y.-Q. Zhang, E.-C. Yang and X.-J. Zhao, Magnetic relaxation dynamics of a centrosymmetric Dy2 single-molecule magnet triggered by magnetic-site dilution and external magnetic field, *Inorg. Chem.*, 2017, **56**, 5611-5622.

.